IOP Publishing Measurement Science and Technology
Meas. Sci. Technol. 31 (2020) 045015 (13pp) https://doi.org/10.1088/1361-6501/ab5b65

# An encoder information-based anomaly detection method for planetary gearbox diagnosis

**Kaixuan Liang[1], Ming Zhao[1], Jing Lin[2], Jinyang Jiao[1] and Chuancang Ding[1]**

[1] Shaanxi Key Laboratory of Mechanical Product Quality Assurance and Diagnostics, School of Mechanical Engineering, Xi'an Jiaotong University, Xi'an 710049, Shaanxi Province, People's Republic of China
[2] Science & Technology on Reliability and Environmental Engineering Laboratory School of Reliability and Systems Engineering, Beihang University, Road No. 37, Haidian District, Beijing, People's Republic of China

E-mail: lkxcarrot@stu.xjtu.edu.cn, zhaomingxjtu@mail.xjtu.edu.cn, linjing@buaa.edu.cn, jjy2015@stu.xjtu.edu.cn and dingchuancang@stu.xjtu.edu.cn

Received 11 August 2019, revised 7 November 2019
Accepted for publication 25 November 2019
Published 15 January 2020

**Abstract**

To keep the reliability of the planetary gearbox, anomaly detection has been widely investigated for its health monitoring. To this end, a novel approach is presented in this paper to extract fault features based on the merits of built-in encoder signals. Considering that collected encoder data is accumulated in angular positions, instantaneous angular acceleration (IAA) is firstly calculated to highlight the characteristic components. And then time synchronization average (TSA) is applied on an estimated multi-period for denoising, which improves the robustness of the TSA to the feature attenuation effect caused by the round-off error of the basic period. In this paper, we explore the distinguishing properties of regular components and the fault anomaly to impose different restraints on them, which is embodied as a periodicity-enhanced model of robust principle analysis. And objective features are further separated by solving this optimization model. The validation analysis of the proposed framework is applied on both the simulation and experimental cases. The results show that the proposed method is of good performance to deal with encoder signals from the planetary gearbox for fault diagnosis.

Keywords: encoder information, anomaly detection, planetary gearbox, signal denoising, periodicity-enhanced robust PCA (PRPCA)

(Some figures may appear in colour only in the online journal)

## 1. Introduction

Planetary gearboxes are widely used in rotating machinery for motion and torque transmission owing to their compact structure and the ability to handle large torque loads [1]. Under the tough working environment, failures are easily generated on the key components, which may give rise to catastrophic accidents and enormous economic losses [2, 3]. To keep the reliability of the planetary gearbox, the acquisition and analysis of status information via effective measurement approaches for health monitoring have long been a hotspot in the research field.

Vibration analysis, as a conventional monitoring approach of mechanical equipment, has reached remarkable achievements in the past several decades [4–6]. However, limited by the installation mode of accelerometers, vibration analysis is not always a reliable and effective way for the diagnosis of a planetary gearbox in industrial applications. The primary

 

reason is that the accelerometer as an external device is prone to the influence of the long transfer path during the measurement, especially in the scenarios of monitoring large-scale machinery. And due to the revolution of planet gear around the sun gear, the gear mesh location is time-varying relative to the fixed vibration sensor, which brings a lot of difficulties for subsequent signal processing.

Along with the development of sensing techniques, a lot of new measurement means have been explored for the health assessment of the gearbox [7–9]. Among them, the rotary encoder has received considerable attention relying on its outstanding advantages: (1) compared with the translational vibration information sampled by the accelerometer, encoder data places more emphasis on the torsional behavior, which is more sensitive to the weak oscillations induced by fault [10–12]; (2) the rotary encoder as a built-in device has easier accessibility than other measuring methods of torsional information, such as a laser torsional vibrometer [13] and torque sensor [14]; and (3) the direct collection of torsional information by a rotary encoder avoids the amplitude modulation effect caused by the changes of transfer path. Motivated by these merits, some approaches of fault detection based on encoder signals have been reported in the literature. For example, by analyzing the shape of rotating speed fluctuations, Bourdon *et al* [15] presented the basic signal processing techniques to quantify taper roller bearing outer race faults according to the instantaneous angular speed (IAS) acquired from the encoder. Li *et al* [16] proposed a new IAS estimation approach and further employed the empirical mode decomposition (EMD) and autocorrelation local cepstrum to extract fault features from IAS for the assessment of a sophisticated multistage gearbox [17]. In [18], Zhou *et al* studied the condition monitoring way of feed-axis gearbox using a built-in motor encoder and linear scale combined with the ensemble EMD method. Zeng *et al* [19] analyzed the IAS signal estimated by an encoder for the diagnosis of the planetary gear fault. In order to explore the intrinsic features of the encoder signal, Jiao *et al* [20] fused multivariate encoder information as the input of convolutional neural network (CNN) for intelligent diagnosis and proved the effectiveness. Besides, in [21–23], researchers have also studied the application of encoder signal on transmission error measurements for the rotating shaft.

The above research achievements have proved that a rotary encoder is qualified to be a valid information source for the health monitoring of rotating machinery. However, some issues are required to be further considered. Firstly, most of the researches focus on the analysis of IAS instead of the instantaneous angular acceleration (IAA), and the latter is linearly related to the torque variation, which can be more effective to detect the torsional anomaly. Secondly, the studies of encoder signal on the planetary gearbox diagnosis are limited, thus further exploration is necessary to be carried out in view of its complex structure and the dispersion of torque transmission. In addition, the existing approaches mainly employ the conventional spectrum analyzing methods or decomposition methods like EMD for fault detection, which is easily disturbed by various interfering components generated in a planetary gearbox. Although [20] introduced an advanced CNN-based method, it is confined to the difficulty of acquiring enormous training data in practical applications. Therefore, aiming at enhancing the practicality of encoder information for the anomaly detection of the planetary gearbox, this paper provides an alternative approach through a way of matrix decomposition. In this work, the IAA signal is denoised by time synchronization average (TSA) on an estimated multi-period to enhance the component with target period. And then a periodicity-enhanced robust principal component analysis (PRPCA) model is constructed and solved to separate the anomaly induced by local fault. The main contributions can be summarized as follows.

(1) The IAA derived from the encoder signal is used as the analysis object, which contributes to saving the cost on measurement and providing a more reliable analysis result.
(2) In order to improve the performance of TSA in the situation that the number of points in each target period is not the integer, a multi-period estimation strategy is designed to avoid the attenuation effect on the useful component.
(3) By transforming the denoised IAA into a matrix form, the constructed PRPCA model makes full use of the essential difference of the components from different origins, i.e. low-rank property of regular part and sparse property of the abnormal part, which leads to an accurate detection of the failure.

The layout of this article is organized as follows. Section 2 elaborates on the framework and details of the proposed approach. In section 3, the guidance for selecting several key parameters is illustrated and verified by a simulation model. In section 4, signals from a planetary gearbox with different fault types are analyzed to prove the validity of the new method. And section 5 finally draws some conclusions.

## 2. Proposed approach

### 2.1. Preprocessing of the encoder signal

The rotary encoder records the discrete position series along with the rotation of shaft, so that the magnitude of fluctuation caused by fault will be of an extremely small quantity compared with the current sampling value. Thus, it is imperative to firstly convert the original encoder signal into some more sensitive variables like IAS, IAA or other higher difference of angular displacement. Among these variables, IAA is linearly related to the torque and directly reflects the dynamic behavior of the shaft. On this account, it is employed as the preliminary feature in this work for anomaly detection of planetary gearboxes.

The calculation of IAA from the sampled encoder signal can be expediently solved by the central difference method (CDM) as

$$a_k = \frac{\varphi_{k+1} - 2\varphi_k + \varphi_{k-1}}{\Delta t^2} \tag{1}$$

where $\varphi_k$ donates the angular position, $a_k$ is the corresponding IAA and $\Delta t$ represents the sampling interval. It is worth noting

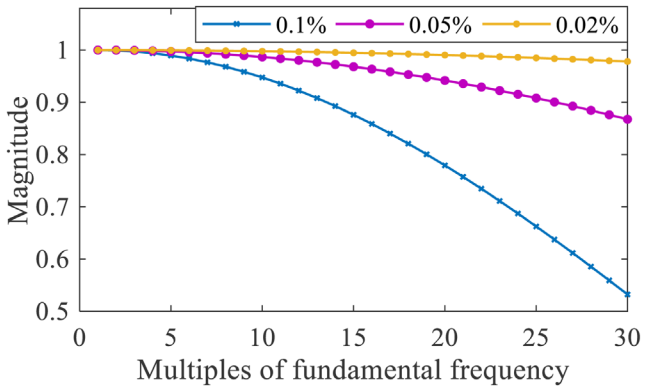


**Figure 1.** Attenuation effect on objective frequencies with different deviation.

that sampling rate has some influence on the accuracy of IAA estimation, which will be discussed in section 4.

### *2.2. Denoising by multi-period time synchronization average (MTSA)*

Due to the fact that the encoder signal is usually influenced by meshing fluctuation, shaft rotation variation, fault anomaly and noise, it is meaningful to heighten the components with a desired period, i.e. the rotation period of the fault gear, and suppress the others. Taking the particularity of the encoder signal into consideration, rotational speed is easily obtained from the control system or estimated via regression approaches such as the least square method (LSM). With this *a priori* knowledge, time synchronous averaging (TSA) is effective to maximize periodic components specifically from the mixture [24]. The expression of TSA in time domain is formulated as

$$\widetilde{a}_n = \frac{1}{N}\sum_{i=0}^{N-1} a_{n+iL} \tag{2}$$

where $N$ denotes the total number of periods to be averaged, and $L$ presents the number of points within each period, which can be approximatively obtained according to the rotational frequency $f_r$ and sample frequency $f_s$, i.e.

$$L_0 = \frac{f_s}{f_r} \tag{3}$$

however, $f_s$ is usually not divisible exactly by $f_r$ in practical scenarios, hence $L_0$ is not guaranteed to be an integer. In fact, TSA is essentially a comb filter extracting the fundamental frequency as well as its multiples [25]. Hence small deviation on the averaging period will cause a large attenuation in the high-frequency section. Figure 1 presents the attenuation effect on objective frequencies when the deviation of the period is set as 0.02%, 0.05% and 0.1% for TSA. It is obvious that the objective components in the high frequency band are sharply reduced along with the deviation increasing. Considering that high frequency response is crucial to describe the transient characters, traditional TSA accordingly loses too much useful information when the round-off error of $L_0$ is large.

Given this issue, we tactfully extend $L$ as an appropriate multiple of $L_0$ to meet an integer approximatively. This extension may reduce the effectiveness of TSA a little but makes up for the round-off error. With this trade-off, the high frequency components can be retained adequately. Literally, this method is called multi-period TSA (MTSA) in this paper, and $L$ is fixed with the following formulation:

$$L = \min_r \ \text{round}(rL_0) \ s.t. \left|\frac{L}{r} - L_0\right| < \frac{\xi}{N} \tag{4}$$

where round$(\cdot)$ denotes round-off operation and $r$ represents the smallest integer satisfying the condition. $\xi$ is a margin to control the synchronism deviation between the first and last period to be averaged, which is suggested to be around one-tenth of the number of sampling points in one meshing. Note that the increasing period length also enlarges the bandwidth of the comb filter, thereby enhancing its robustness to slight speed fluctuation.

### *2.3. Construction of the PRPCA model*

Despite MTSA eliminating most of the noise, some challenges still exist. The deficiency of the gear mainly causes the variations of meshing stiffness, which is insufficient to evoke the distinct amplitude impulses among the rest interferences in the initial stage, hence further analysis is required to separate the abnormal part. And the complex structure of the planetary gearbox also gains the coupling of various components. Further, sometimes the occurrence of multi-fault will disturb the regularity of the frequency spectrum. Taking all of these into consideration, the commonly used time and frequency domain analysis methods are incompetent to separate the discriminating information.

And yet for that, a new way is explored to extract the fault feature by focusing on the peculiar attribute of different components. Specifically, it is well understood any two sections of the regular interferences, such as meshing oscillation, within a period are usually of a strong correlation. From the matrix perspective, this correlation can be mathematically described as the low-rank property. As for the fault features, they are just individual transients distributed in each period, which can be conveniently constrained as a sparsity term. On this basis, an operator $R$ is firstly defined to transform the denoising signal into its matrix form:

$$\mathbf{M} = R(\widetilde{\mathbf{a}}) = \begin{bmatrix} \widetilde{a}_1 & \widetilde{a}_2 & \cdots & \widetilde{a}_{N-m+1} \\ \widetilde{a}_2 & \widetilde{a}_3 & \cdots & \widetilde{a}_{N-m+2} \\ \vdots & \vdots & \ddots & \vdots \\ \widetilde{a}_m & \widetilde{a}_{m+1} & \cdots & \widetilde{a}_N \end{bmatrix} \tag{5}$$

where each column of $\mathbf{M}$ is a portion of the result from MTSA with length $m$. To reduce variability, $\mathbf{M}$ is normalized by dividing its Frobenius norm.

Based on above descriptions, the components from different sources are able to be specifically restricted, and then $\mathbf{M}$ can be divided into two distinct matrices, i.e. the regular components $\mathbf{L}$ and sparse components $\mathbf{S}$, by the following optimization model:

$$\min_{\mathbf{L},\mathbf{S}} \text{rank}(\mathbf{L}) + \lambda\|S\|_0 \ s.t. \ \mathbf{M} = \mathbf{L} + \mathbf{S} \tag{6}$$

where $\|\cdot\|$ denotes the $l_0$-norm and $\lambda > 0$ is a trade-off parameter.

Regarding equation (6), it is a typical form of robust principal component analysis (RPCA) model, which is widely researched on background modeling and shadow removing [26]. Despite that the optimization of low-rank and $l_0$-norm has been proven to be NP-hard, it is proved that the rank and $l_0$-norm restrictions can be relaxed to their convex envelopes under rather broad conditions [27], which is expressed as follows:

$$\min_{\mathbf{L},\mathbf{S}} \|\mathbf{L}\|_* + \lambda\|\mathbf{S}\|_1, \ s.t.\ \mathbf{M} = \mathbf{L} + \mathbf{S} \tag{7}$$

where $\|\cdot\|_*$ is the nuclear norm equaling the sum of singular values of the input matrix and $\|\cdot\|_1$ is the sum of the absolute values of matrix entries. It should be paid attention that the above convex relaxation operation also increases the tolerance of this model to residual noise since $\mathbf{L}$ is not strictly limited as a low-rank matrix. And in order to extract the fault anomaly more purely, a periodicity-enhanced model named PRPCA is further proposed, which rewrites equation (7) as

$$\min_{\mathbf{L},\mathbf{S}_0} \|\mathbf{L}\|_* + \lambda\|\mathbf{C}\mathbf{S}_0\|_1, \ s.t.\ \mathbf{M} = \mathbf{L} + \mathbf{C}\mathbf{S}_0 \tag{8}$$

where $\mathbf{C} = [\mathbf{E},\ldots,\mathbf{E}]^T$ and $\mathbf{E} \in \mathbb{R}^{\tilde{L}_0 \times \tilde{L}_0}$ is an identity matrix. $\tilde{L}_0$ represents the rounded $L_0$. Compared with equation (7), equation (8) replaces $\mathbf{S}$ as a repeating extension of $\mathbf{S}_0 \in \mathbb{R}^{\tilde{L}_0 \times (N-m+1)}$, i.e.

$$\mathbf{S} = \begin{bmatrix} \mathbf{S}_0 \\ \vdots \\ \mathbf{S}_0 \end{bmatrix} \tag{9}$$

where $m = N_c\tilde{L}_0$ is adopted and $N_c$ is an integer suggested as 2 or 3 in order not to be influenced by the round-off error of the period. By this, the sparse features in each column of $\mathbf{S}$ is constrained to be strictly periodic in the local, which is conducive to the better separation of fault anomaly in calculation.

### 2.4. Solution to PRPCA model

Many approaches have been proposed to solve the RPCA model [27–29]. Among these, the augmented Lagrange multipliers (ALM) method is widely used due to its superior performance on both the convergence speed and precision [29]. As a variant of the RPCA model, the proposed PRPCA model can be also solved by ALM, which converts equation (8) as

$$\min_{\mathbf{L},\mathbf{S}_0} \|\mathbf{L}\|_* + \lambda\|\mathbf{C}\mathbf{S}_0\|_1 + \langle\Lambda, \mathbf{M} - \mathbf{L} - \mathbf{C}\mathbf{S}_0\rangle + \frac{\mu}{2}\|\mathbf{M} - \mathbf{L} - \mathbf{C}\mathbf{S}_0\|_F^2 \tag{10}$$

where $\mathbf{\Lambda}$ is the Lagrangian operator matrix, $\langle\cdot,\cdot\rangle$ is the sum of product of the corresponding elements. $\|\cdot\|_F$ denotes Frobenius norm and $\mu$ signifies the regularization term parameter. In order to find the minima for $\mathbf{L}$ and $\mathbf{S}_0$, the alternating optimization is adopted, and then equation (10) can be divided into the following two subproblems.

$$\mathbf{L}_k = \arg\min_{\mathbf{L}_k} \|\mathbf{L}_k\|_* + \frac{\mu}{2}\|\mathbf{L}_k - (\mathbf{M} - \mathbf{C}\mathbf{S}_{0,k-1} + \mathbf{\Lambda}_{k-1}/\mu)\|_F^2 \tag{11}$$

$$\mathbf{S}_{0,k} = \arg\min_{\mathbf{S}_{0,k}} \lambda\|\mathbf{C}\mathbf{S}_{0,k}\|_1 + \frac{\mu}{2}\|\mathbf{C}\mathbf{S}_{0,k} - (\mathbf{M} - \mathbf{L}_k + \mathbf{\Lambda}_{k-1}/\mu)\|_F^2 \tag{12}$$

$$\mathbf{\Lambda}_k = \mathbf{\Lambda}_{k-1} + \mu(\mathbf{M} - \mathbf{C}\mathbf{S}_{0,k} - \mathbf{L}_k). \tag{13}$$

The detailed derivative process of equations (11) and (12) is given in the appendix. Regarding the periodicity operator $\mathbf{C}$ in equation (12), another matrix $\mathbf{A} \in \mathbb{R}^{\tilde{L}_0 \times m}$ is constructed for the computational convenience:

$$\mathbf{A} = \frac{1}{N_c}[\mathbf{E}, ..., \mathbf{E}]. \tag{14}$$

It is easily obtained that $\mathbf{AC} = \mathbf{E}$. Then equation (12) can be rewritten as

$$\mathbf{S}_{0,k} = \arg\min_{\mathbf{S}_{0,k}} \lambda\|\mathbf{S}_{0,k}\|_1 + \frac{\mu}{2}\|\mathbf{S}_{0,k} - \mathbf{A}(\mathbf{M} - \mathbf{L}_k + \mathbf{\Lambda}_{k-1}/\mu)\|_F^2. \tag{15}$$

The translation from equation (12) to (15) can be demonstrated by focusing on their element-wise computation, i.e.

$$\begin{aligned}\mathbf{S}_{0,k} &\leftarrow \arg\min_{\mathbf{S}_{0,k}} \sum_{i=1}^{\tilde{L}_0}\sum_{j=1}^{N-m+1}\left\{N_c\lambda|s_{ij}| + \frac{\mu}{2}\sum_{r=0}^{N_c-1}\left(s_{ij} - e_{(i+r)j}\right)^2\right\} \\ &= \arg\min_{\mathbf{S}_{0,k}} \sum_{i=1}^{\tilde{L}_0}\sum_{j=1}^{N-m+1}\left\{\lambda|s_{ij}| + \frac{\mu}{2}\left(s_{ij} - \frac{1}{N_c}\sum_{r=0}^{N_c-1} e_{(i+r)j}\right)^2\right\}\end{aligned} \tag{16}$$

where $s_{ij}$ and $e_{(i+r)j}$ represent the elements of $\mathbf{S}_{0,k}$ and $\mathbf{E}_k = \mathbf{M} - \mathbf{L}_k + \mathbf{\Lambda}_{k-1}/\mu$ respectively. The right part of equation (16) is exactly the expansion of equation (15).

Although equations (11) and (15) cannot to be directly solved in a derivative way because that nuclear norm and $l_1$-norm are not strictly differentiable, [30] provides a particular path to solve this problem by introducing a shrinkage operation $T_\tau$ to achieve the convex optimization. Referring to [30], the closed-form solution of equations (11) and (15) can be respectively expressed as

$$\mathbf{L}_k = \mathbf{U}T_{1/\mu}(\mathbf{\Sigma})\mathbf{V}^T \tag{17}$$

$$\mathbf{S}_{0,k} = T_{\lambda/\mu}(\mathbf{A}(\mathbf{M} - \mathbf{L}_k + \mathbf{\Lambda}_{k-1}/\mu)) \tag{18}$$

where $\mathbf{U\Sigma V}^{\mathrm{T}}$ is the singular value decomposition (SVD) of $\mathbf{M} - \mathbf{C}\mathbf{S}_{0,k-1} + \mathbf{\Lambda}_{k-1}/\mu$ and $T_\tau$ is a soft thresholding operator defined as

$$T_\tau(a) = \begin{cases} a - \tau \mathrm{if} x > \tau \\ a + \tau \mathrm{if} x < -\tau \\ 0 \mathrm{otherwise} \end{cases}. \tag{19}$$

The algorithm flow of solving the PRPCA model is visualized in Algorithm 1, where the model parameters will be discussed in section 3.

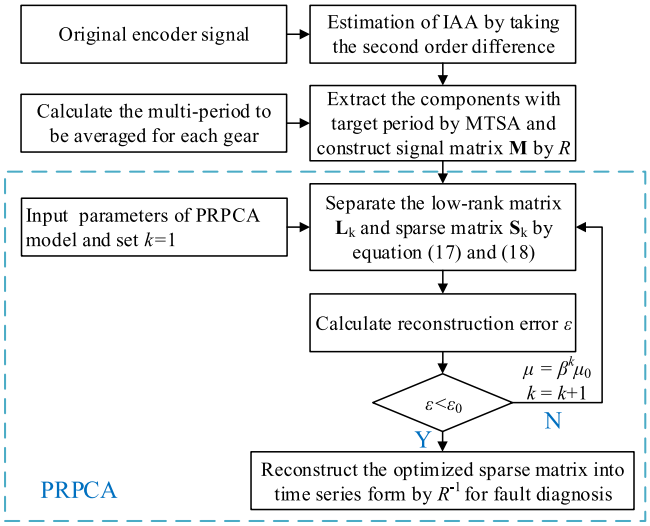


**Figure 2.** The flowchart of the proposed approach.

**Algorithm 1:** The algorithm of solving the PRPCA model via the ALM method

**Input:** Signal matrix **M**

1: Initialize $\mathbf{L}_0 = \mathbf{0}$; $\mathbf{S}_{0,0} = \mathbf{0}$; $\mathbf{\Lambda}_0 = \mathbf{0}$; $\mu > 0$; $\gamma > 1$; $k = 1$.
2: Repeat until the end condition is satisfied:
3: $\mathbf{U}, \mathbf{\Sigma}, \mathbf{V} = \mathrm{SVD}(\mathbf{M} - \mathbf{CS}_{0,k-1} + \mathbf{\Lambda}_{k-1}/\mu)$.
4: $\mathbf{L}_k = \mathbf{U} T_{1/\mu}(\mathbf{\Sigma}) \mathbf{V}^{\mathrm{T}}$.
5: $\mathbf{S}_{0,k} = T_{1/\mu}(\mathbf{A}(\mathbf{M} - \mathbf{L}_k + \mathbf{\Lambda}_{k-1}/\mu))$.
6: Update $\mathbf{\Lambda}_k = \mathbf{\Lambda}_{k-1} + \mu(\mathbf{M} - \mathbf{L}_k - \mathbf{CS}_{0,k})$.
7: $k = k + 1$.

**Output:** $\mathbf{S}_k = \mathbf{CS}_{0,k}$.

A satisfying solution for the optimized sparse matrix $\hat{\mathbf{S}}$ can be adaptively obtained through implementing Algorithm 1. Thereafter, an inverse process of $R$, named $R^{-1}$, is carried out to recover $\hat{\mathbf{S}}$ into sequence form.

$$\mathbf{x} = R^{-1}(\hat{\mathbf{S}}) = R^{-1}\left(\begin{bmatrix} x_1 & x_2 & \cdots & x_{N-m+1} \\ x_2 & x_3 & \cdots & x_{N-m+2} \\ \vdots & \vdots & \ddots & \vdots \\ x_m & x_{m+1} & \cdots & x_N \end{bmatrix}\right) = [\bar{x}_1, \bar{x}_2, \bar{x}_3, ..., \bar{x}_N] \tag{20}$$

where $\bar{x}_j, j \in [1, N]$ represents the averaged value of the variables with the same subscript and **x** is the reformed sparse feature.

### 2.5. General framework of the proposed approach

In order to achieve the monitoring of each target gear, the framework of the proposed method is presented in this section for the separation of fault anomaly. As stated previously, MTSA is employed to denoise IAA, then PRPCA is carried out and solved by an iterative algorithm to extract periodic transients. The flowchart of the proposed approach is shown in figure 2 and the general procedure is summarized as follows:

**Step1:** The encoder signal is sampled and converted to IAA signal by taking its second-order difference.

**Step2:** By estimating the multi-period for synchronous average according to equation (4) for each gear, MTSA is employed for enhancing the target components, and the results are then transformed as a matrix.

**Step3:** PRPCA is implemented to separate the sparse fault features and recover it back to the time series form.

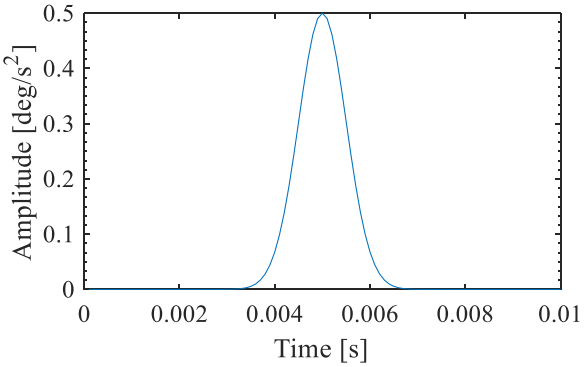


**Figure 3.** Fault anomaly formulated by the Gaussian function.

## 3. Simulation analysis

### 3.1. Simulation signal generation

A simulation model of the encoder signal is constructed in this section to investigate the validity of the proposed method for gearbox transmission monitoring. Different from vibration data, the angular positions collected by the rotary encoder are cumulative in the sampling process. In the case of keeping revolving speed constant, the encoder signal is expected to be an approximate linear curve that is disturbed by meshing oscillation, transient impulses and noise, etc. Therefore, the encoder signal could be generally expressed as the following form [31]:

$$\begin{aligned} \varphi(t) &= v_0 t + \sum_k A_k \cos(2\pi f_k t + \phi_k) + \sum_i g(t - iT_0) + w_\sigma(t) \\ g(t) &= B \exp(-t^2/2\tau^2) \end{aligned} \tag{21}$$

where the first term denotes cumulative angular positions of rotating shaft under a constant speed $v_0$. The second term includes position oscillation due to load variation and the interference caused by rotating parts as well as gear meshing, where $A_k$ denotes the amplitude, $f_k$ and $\phi_k$ are the frequency and phase respectively. The third term represents the periodic anomaly during the transmission induced by the mechanical deficiency with a period of $T_0$, where $g(t)$ is a Gaussian function as presented in figure 3, which is employed to simulate the anomaly caused by fault. The last part $w_\sigma(t)$ stands for the background noise with the standard deviation of $\sigma$.

Figure 4 displays the waveforms of the simulated encoder signal within 2 s. The sampling rate is set as 5000 Hz and the other parameters are listed in table 1. It can be found that the original encoder signal in figure 4(a) is almost linear where no useful information can be directly observed. After taking the second-order difference as presented in figure 4(b), the IAA of the mixed signal is still chaotic because some of the interferences are magnified simultaneously along with fault anomaly, which requires further processing to extract distinguishing features.

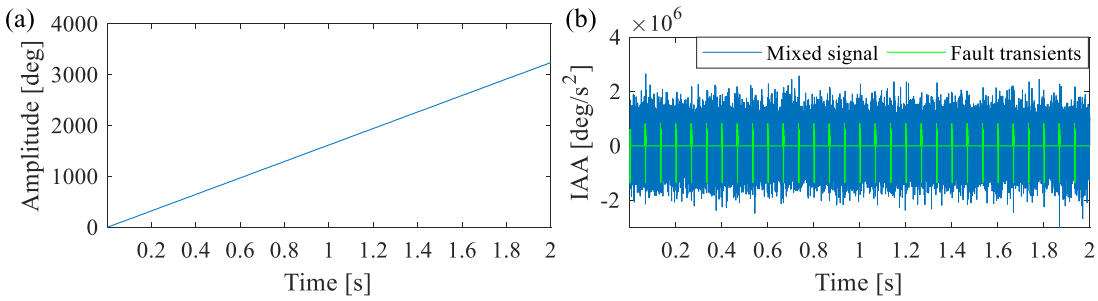


**Figure 4.** (a) Original encoder signal. (b) IAA of mixed signal and fault anomaly.

**Table 1.** The parameters for encoder signal simulation.

| Parameters | Value | Parameters | Value |
|---|---|---|---|
| $v_0$ (rpm) | 270 | $f_2$ (Hz) | 4.5 |
| $B$ (degree) | 0.5 | $A_2$ (degree) | 0.8 |
| $\tau$ (s) | 0.0003 | $\phi_2$ (rad) | $\pi/4$ |
| $T_0$ (s) | 1/13 | $f_3$ (Hz) | 273 |
| $f_1$ (Hz) | 20 | $A_3$ (degree) | 0.3 |
| $A_1$ (degree) | 1 | $\phi_3$ (rad) | 0 |
| $\phi_1$ (rad) | $\pi/2$ | $\sigma$ (degree) | 0.02 |

### *3.2. Parameters analysis*

*3.2.1. Estimation of model parameters.* In the implementation of PRPCA, there are two key model parameters, i.e. $\mu$ and $\lambda$ should be carefully considered because they are important to the convergence speed and discrimination of the result. The value of $\mu$ is fixed differently in various applications [26, 29, 32]. Despite this fact, [29] had verified that the RPCA algorithm will converge faster with growing $\mu$ in a geometrically speed. Based on this conclusion, we get

$$\mu_k = \beta^k \mu_0 \tag{22}$$

where $\beta$ is a factor to control the growth rate, $\mu_0$ is set as the initial value and $k$ is the current iteration number. Since $\mu$ is growing geometrically, the value of $\beta$ and $\mu_0$ is suggested as 1.1 and $1.25/\|\mathbf{M}\|_2$ respectively.

The selection of $\lambda$ is also important since it balances the proportion between te low-rank part and sparse part. A large $\lambda$ will apparently increase the sparsity of $\mathbf{S}$ and even lead to a null matrix. In most of aforementioned achievements, this parameter is either fixed by experience or approximatively chosen as

$$\lambda = \frac{1}{\sqrt{\max(m, N-m+1)}} \tag{23}$$

however, concluding from redundant assumptions and a complicated proving process, it is hard to understand why equation (23) works in the applications. In light of this, a suggested value of $\lambda$ is deduced from the solving process of PRPCA in this paper, which also provides a brief guidance to suitably adjust its assignment in practice.

In view of the iterative calculation of equations (17) and (18), the latter can be rewritten as

$$\mathbf{S}_{0,k} = \mathbf{T}_{\lambda/\mu}(\mathbf{AG} + \mathbf{S}_{0,k-1}) \tag{24}$$

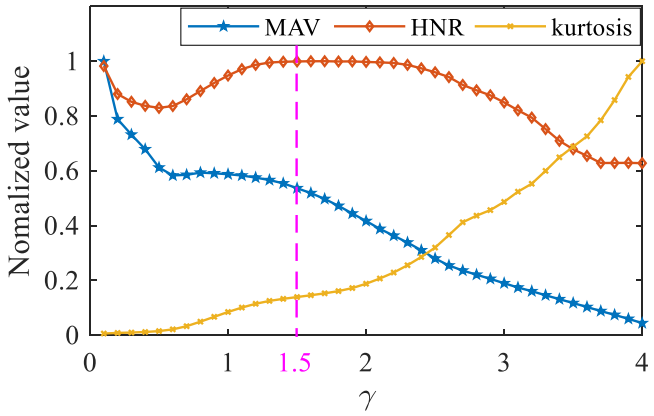


**Figure 5.** The MAV, HNR and kurtosis of the extracted sparse feature under different $\gamma$.

where $\mathbf{G} = \mathbf{M} - \mathbf{CS}_{0,k-1} + \mathbf{\Lambda}_{k-1}/\mu - \mathbf{L}_k$ is an intermediate matrix in the alternate iteration between $\mathbf{L}_k$ and $\mathbf{S}_k$. Combined with equation (17), it is easily obtained that

$$\|\mathbf{G}\|_F^2 = \alpha \frac{\min(m, N-m+1)}{\mu^2}. \tag{25}$$

where $\alpha$ is a scale factor decided by the distribution of singular values within $\mathbf{\Sigma}$. The concrete value of $\alpha$ is hard to compute in the iteration, and it equals 1 only when all these singular values are no less than $1/\mu$. Experimentally, a value close to 1 but a little smaller is available for $\alpha$ in most cases.

Assume that all the entries of $\mathbf{G}$ share a common value under the constraint of equation (25) only, it is readily obtained that the elements of $\mathbf{G}$ can be expressed as

$$\eta = \frac{\sqrt{\alpha}}{\mu\sqrt{\max(m, N-m+1)}} \tag{26}$$

however, for the reason that $\mathbf{G}$ is never a matrix as the assumption, the sparse entries with high amplitude in $\mathbf{G}$ are naturally larger than $\eta$.

Then, equation (24) can be focused to find the best estimation of $\lambda$. After the averaging of $\mathbf{A}$, the elements in $\mathbf{G}$ with local periodicity and high amplitude will be kept beyond $\eta$, where most of the rest are expected to be less than $\eta$. Thus it is reasonable to assign the soft threshold $\lambda/\mu$ in equation (24) as $\eta$, which will reserve the periodic sparse features into $\mathbf{S}_{0,k}$ and eliminate the small disturbances simultaneously. Thus,

$$\lambda = \frac{\gamma}{\sqrt{\max(m, N-m+1)}} \tag{27}$$

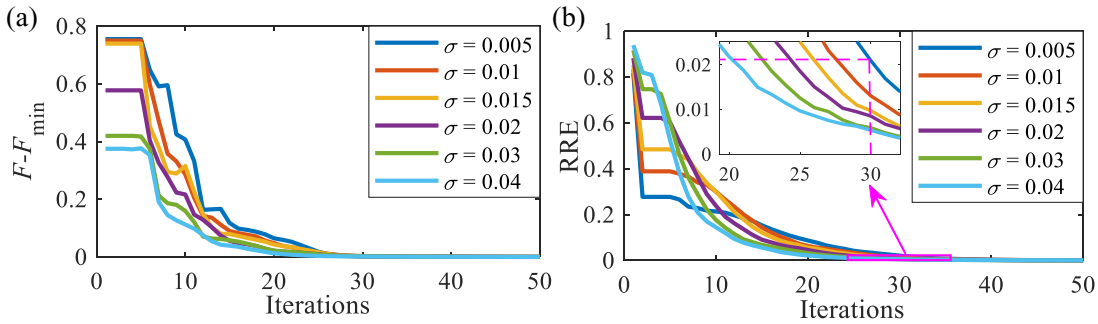


**Figure 6.** The indicators of convergence process under different levels of noise: (a) $F - F_{\min}$, (b) RRE.

where $\gamma$ is an adjustment factor that is selected a little larger than $\sqrt{\alpha}$ to improve the sparsity of the result.

The proposed MTSA-PRPCA method is then analyzed based on the parameters and simulation model discussed above. In this simulation, $\gamma$ is set in the range from 0.1 to 4 with an interval of 0.1 and three indicators, i.e. kurtosis, harmonic-to-noise ratio (HNR) [33] and maximum absolute value (MAV), are employed to reflect the properties of the results. All the three indicators are plotted in figure 5 after a normalization by dividing their maximum. Obviously, with the increase of $\gamma$, the sparsity of the results becomes more significant, which can be realized by observing the tendency of MAV and kurtosis. On the other hand, the change of HNR shows the weight variation of the periodic component. Since the desired result is expected to be periodic and sparse but with a relatively large amplitude, the value of $\gamma$ is suggested in the range of 1.3–2.3 and 1.5 is finally adopted.

*3.2.2. Stopping criterion for iteration in PRPCA.* As for the stopping criterion of PRPCA, two ways are available in traditional RPCA to provide the alternatives, i.e. the threshold value of relative reconstruction error (RRE) and the total number of iterations. RRE is actually a normalized variable defined as

$$\varepsilon = \frac{\|\mathbf{M} - \mathbf{L}_k - \mathbf{S}_k\|_F}{\|\mathbf{M}\|_F}. \tag{28}$$

Obviously, RRE is directly relevant to the degree of convergence. And by contrast, the fixed number of iterations seems to be inflexible. In this subsection, the simulated signals with different levels of noise are studied to find the applicable stopping criterion. In order to observe the convergence process, we firstly define the normalized value of the objective optimization function in equation (8) as $F(k)$:

$$F(k) = \frac{\|\mathbf{M} - \mathbf{CS}_{0,k}\|_* + \lambda\|\mathbf{CS}_{0,k}\|_1}{\|\mathbf{M}\|_F}. \tag{29}$$

The convergence process of simulated signals is illustrated in figure 6, where $F$ is plotted by subtracting its minimum value under each $\sigma$ for the convenience of comparison. It can be found that $F$ nearly converges to the minimum after 30 iterations for all the signals, which means that the satisfied results are already obtained and further calculation is meaningless. From the curves of RRE as presented in figure 6(b), the magnitudes of RRE at 30 iterations are around $10^{-2}$. Since the noise used in the simulation is in a fairly wide range, the stopping criterion can be accordingly set as 0.01 of RRE in the execution of PRPCA.

### 3.3. Performance of MTSA-PRPCA

To show the robustness of the proposed approach to random noise, the simulated signals with different standard deviation of noise are further analyzed. Figure 7 depicts the analysis results obtained by CDM, MTSA and MTSA-PRPCA under three representative levels of noise, i.e. the standard deviation of 0.005, 0.015 and 0.04. It can be seen from figure 7(a) that the fault anomaly is difficult to identify after CDM due to the existence of noise. In figure 7(b), even that most of the noise is removed by MTSA, the useful features are still not evident in figures 7(b)-2 and (b)-3. And yet for that, by virtue of PRPCA, the fault anomaly is faultlessly separated under all the three levels of noise as shown in figure 7(c), which validates its excellent performance for periodic anomaly extraction.

## 4. Experimental validation

In order to present the validity of the proposed method in practical applications, different types of tooth defect on a planetary gearbox are introduced for the analysis in this experiment. The experimental setup is shown in figure 8(a), which consists of a servo motor, a magnetic break for loading and a planetary gearbox with an internal structure as given in figure 8(b). Besides, two Heidenhain rotary encoders with 5000 pulses per revolution are equipped on this experiment rig to measure the angular displacements of input shaft and output shaft respectively. In this paper, the output encoder signals were collected for analysis by an IK220 counter card at a sampling rate of 5000 Hz.

The computational formulas of characteristic frequencies (CFs) are listed in table 2, where $N_p = 3$ is the number of planet gears equally spaced in the gearbox, $f_i$ represents input frequency and $Z_p$, $Z_s$, $Z_r$ denote the number of teeth on planet gear, sun gear and ring gear, respectively. The data was acquired in 2 s with the input frequency of 30 Hz and corresponding CFs are displayed in table 3, where the corresponding periods of planet gear, sun gear, ring gear and gear meshing are presented in table 4. The total deviation $\xi$ is calculated as 1.037 point in order not to lose too much fault

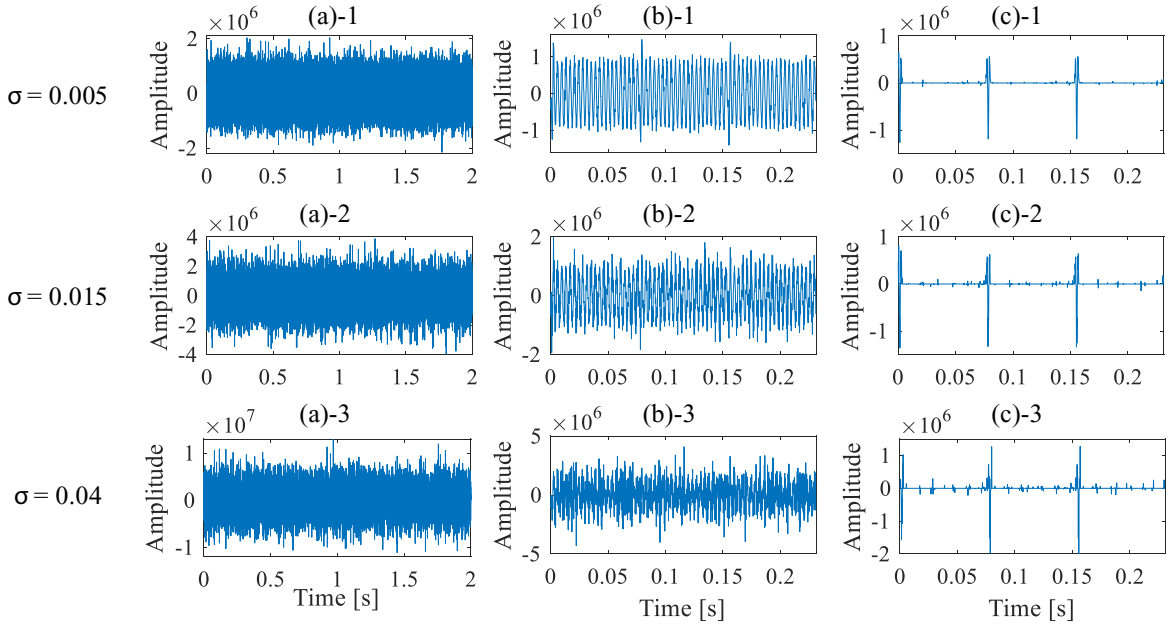


**Figure 7.** The analysis results under a different level of noise: (a) IAA obtained by CDM, (b) IAA denoised by MTSA, (c) fault anomaly separated by MTSA-PRPCA.

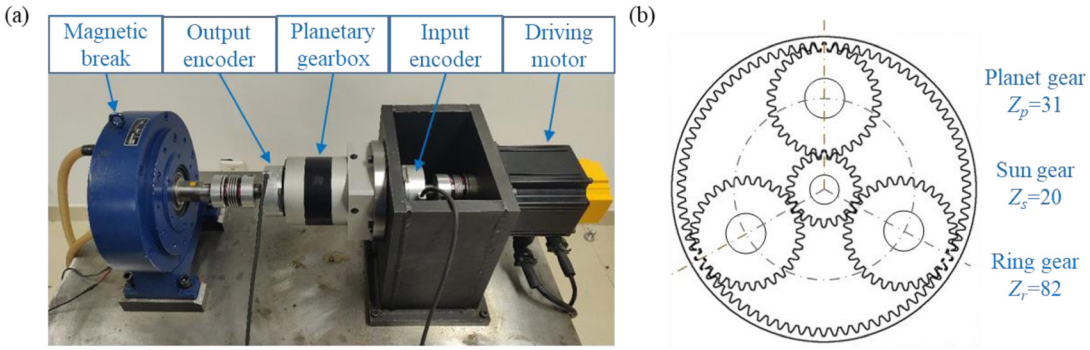


**Figure 8.** (a) Experimental setup, (b) schematic structure of the planetary gearbox.

**Table 2.** Computational formulas of CFs.

| Terms | Formulas |
|---|---|
| Output frequency | $f_o = f_i/T_r$ |
| Meshing frequency | $f_m = f_i \cdot \frac{Z_r Z_s}{Z_r+Z_s}$ |
| Characteristic frequency of planet gear | $f_p = f_m/Z_p$ |
| Characteristic frequency of sun gear | $f_p = f_m/Z_s \cdot N_p$ |
| Characteristic frequency of ring gear | $f_r = f_m/Z_r \cdot N_p$ |

**Table 3.** The CFs with input frequency of 30 Hz.

| CFs | $f_i$ | $f_o$ | $f_m$ | $f_p$ | $f_s$ | $f_r$ |
|---|---|---|---|---|---|---|
| Values (Hz) | 30 | 5.88 | 482.35 | 15.56 | 72.35 | 17.65 |

**Table 4.** Basic periods of characteristic components.

| Periods | Gear meshing ($T_m$) | Planet gear ($T_p$) | Sun gear ($T_s$) | Ring gear ($T_r$) |
|---|---|---|---|---|
| Values (points) | 10.37 | 321.34 | 69.10 | 283.33 |

**Figure 9.** The cracked tooth on planet gear.

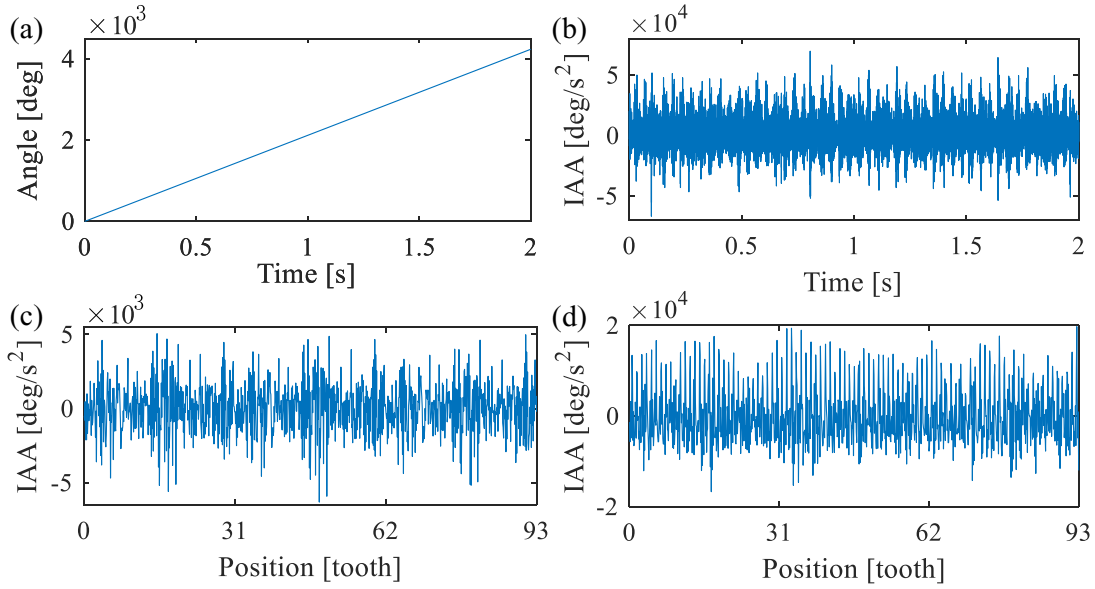


**Figure 10.** (a) Raw encoder signal, (b) IAA obtained by CDM, (c) IAA denoised by TSA, (d) IAA denoised by MTSA.

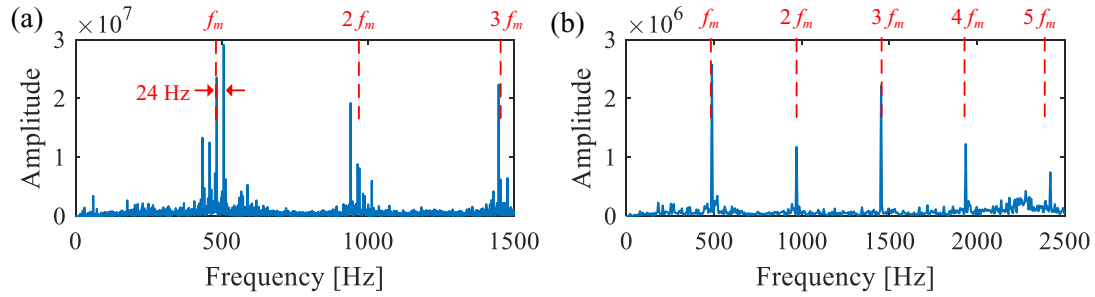


**Figure 11.** The frequency spectrum of (a) IAA obtained by CDM and (b) IAA denoised by MTSA.

information. Derived from equation (4), the extensional multiples of $T_p$, $T_s$, $T_r$ in MTSA are 3, 10 and 3, respectively.

### *4.1. Case 1: cracked tooth on the planet gear*

Due to the harsh working conditions and periodic alternating load, tooth crack is a common failure type, which usually occurs at the root of the gear. The development of crack will eventually cause the breakage of teeth or even the entire gear. To detect this fault, the proposed approach is first validated on a planet gear as illustrated in figure 9 where an artificial cracked tooth is introduced to generate fault signatures.

Figure 10(a) presents the original raw encoder signal from the setup. Similar to the simulation, it is clearly found that the accumulation of angular displacements is predominant due to its character of monotonically increasing, while the other features are totally indiscernible. To highlight distinguishing details, CDM is implemented to compute the second-order difference signal, which is shown in figure 10(b). However, since the noise is synchronously magnified as well as the meshing variation, slight fluctuations originated from the crack are intractable to be identified from original IAA. To cope with this issue, MTSA is employed on the estimated multi-period for denoising, and direct TSA on rounded basic period is performed as a comparison. From the result in figure 10(c), one can find that the denoised signal by TSA is mussy. Comparatively, the result of MTSA, as presented in figure 10(d), exhibits clear meshing impulses on the location of each tooth even that the round-off error of the basic period exists. And TSA on the single period apparently fails to achieve this. Moreover, amplitudes of the results also reveal that MTSA reserves a more objective component than direct TSA. Note that the result of MTSA is still dominated by the irrelevant components where the weak fault features can hardly be seen. Thus further operation is required to recognize the fault characteristics.

FFT is firstly used to analyze the frequency-domain characteristics of IAA. In figure 11(a), the frequency band from 0 to 1500 Hz is shown to present the clear spectrum, where the large amplitudes can be observed around the meshing frequency as well as its multiples. However, these prominent frequencies are irrelevant with the fault signature, and figure 11(b) reveals that fault information is deeply buried in the meshing components. In order to highlight the superiority of the proposed algorithm, PRPCA and original RPCA are both employed to analyze the denoising signal from MTSA in this case. Figures 12(a) and (b) plot the analysis results by MTSA-RPCA and MTSA-PRPCA, where the matrix is constructed with $N_c = 2$. As discussed previously, PRPCA enhances the local periodicity in the computation, which means it focuses

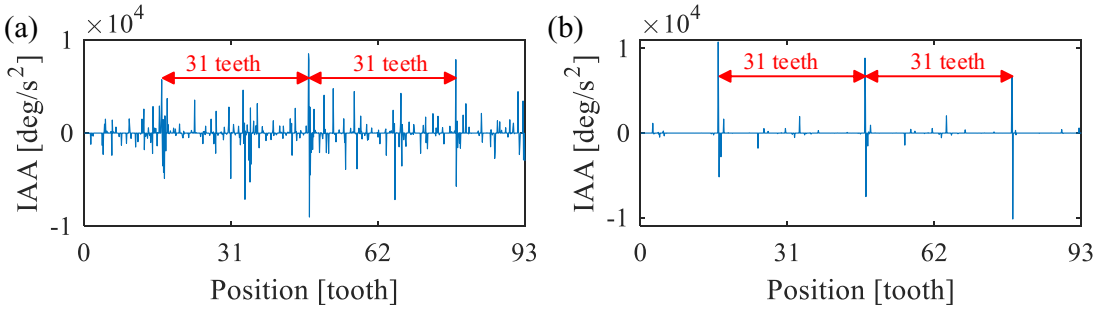


**Figure 12.** Sparse feature obtained by (a) MTSA-RPCA and (b) MTSA-PRPCA.


**Figure 13.** The worn surfaces with interval of 13 teeth on the planet gear.

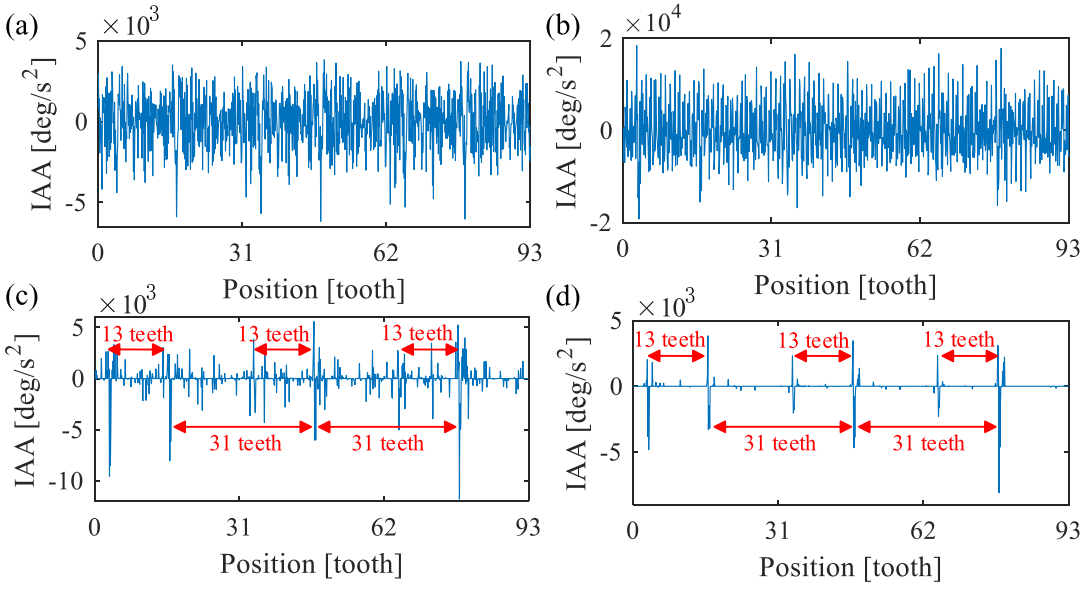


**Figure 14.** IAA denoised by (a) TSA, (b) MTSA and sparse features obtained by (c) MTSA-RPCA and (d) MTSA-PRPCA.

more on identifying periodic sparse transients rather than the ones only with sparsity. This is well validated from the result in figure 12(b) that the equally spaced sparse transients are distinctly viewed. And the internal of 31 teeth coincides with the local fault on the planet gear. For comparison, the result from original RPCA suffers from the residual interferences, which shows the advantage of PRPCA on extracting target fault signatures.

### *4.2. Case 2: surface wear on two teeth*

Surface wear of the tooth is another common failure contributing to the insufficient fatigue strength. In the manufacturing industry,

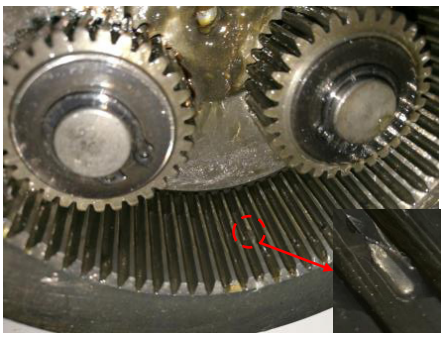

**Figure 15.** The spalled tooth on the ring gear.

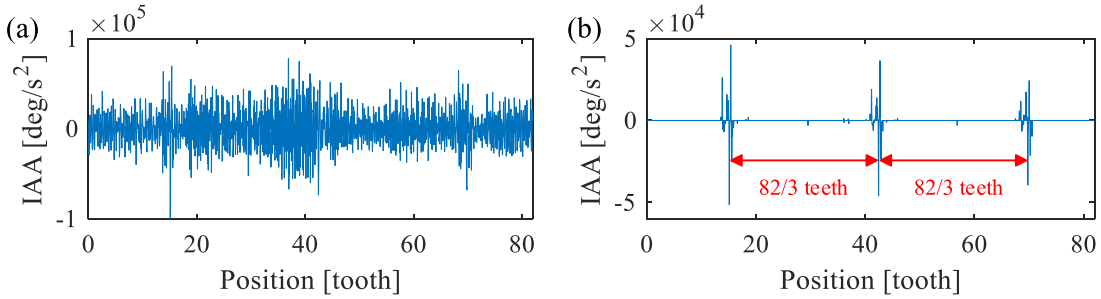


**Figure 16.** (a) IAA denoised by MTSA, (b) sparse feature obtained by MTSA-PRPCA.

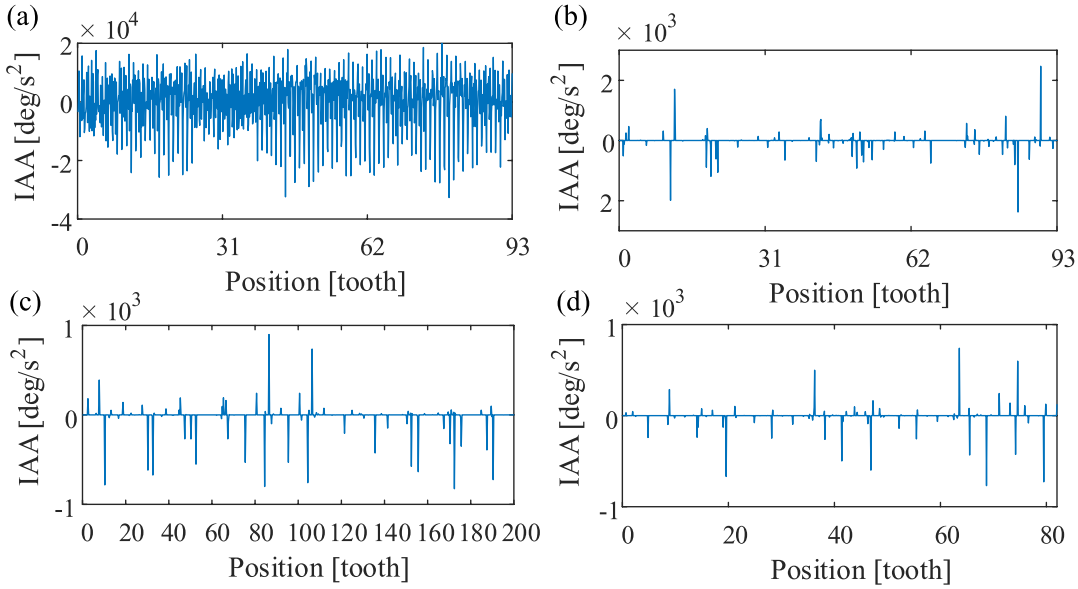


**Figure 17.** (a) IAA denoised by MTSA, and extracted sparse feature for (b) planet gear, (c) sun gear and (d) ring gear.

surface wear will affect machining accuracy, which may cause the scrap of parts. In this case, two teeth with an interval of 13 teeth on the gear are artificially worn to validate the applicability of the proposed method. The gear is shown in figure 13.

Figures 14(a) and (b) present the results of TSA and MTSA, from which we can find that MTSA reserves much more information about the gear meshing no matter on the amplitude or the regularity. Then, PRPCA and RPCA are both used to extract the anomaly as a comparison. Theoretically two distinct impulses are expected to appear within each cycle, however, this is not completely achieved by RPCA from figure 14(c) where interferences disturb the recognition of fault impulses of small amplitude. By embedding the local periodicity, PRPCA presents its superior ability on extracting complete fault information, which can be seen in figure 14(d). The three pairs of impulse spaced by 13 teeth coincide with the defects on the gear. This provides the evidence that PRPCA is prone to periodic anomaly only.

### *4.3. Case 3: spalled tooth on ring gear*

Ring gear is usually an integrated part in the gearbox casing and it is non-replaceable during the whole life cycle of the gearbox. In this subsection, an experiment in terms of spalled tooth failure on the ring gear is invested. The damaged ring gear is exhibited in figure 15. After the difference operation, some abnormal components can be observed from the IAA signal, which is shown in figure 16(a). However, we can hardly conclude that the ring gear is broken according to these exceptions because of the existence of environmental factors, such as the fluctuation of load and external knocks. Figure 16(b) displays the result obtained by MTSA-PRPCA, there is no doubt that the anomaly induced by fault is detected successfully. Since there are three planet gears in the gearbox, the spalled tooth is meshed three times within a cycle and each generates an impulse, which validates the correctness of the result.

### *4.4. Case 4: healthy gearbox*

The encoder signal collected during the operation of a healthy gearbox is also analyzed as a comparison. The IAA denoised by MTSA and final analysis results on the target periods of each gear are presented in figure 17. It is noticed that the sparse features are mainly the random interferences with tiny amplitude and the distinct feature with target period is hardly to be observed, which indicates that the planetary gearbox is under a healthy condition. Therefore, it can be concluded that MTSA-PRPCA is an effective approach for the health identification of the planetary gearbox.

### *4.5. Discussion*

The experiment conducted in our work is under the sampling rate of 5000 Hz where the ratio between sampling rate and meshing frequency (SMR), i.e. the number of sampling points on each tooth meshing, is 10.37 on average. Although the selection of sampling rate will make some difference on IAA due to the discreteness of data, a sufficient analytical accuracy can be obtained by the merits of MTSA-PRPCA in this work, which provides a basic reference that SMR is suggested to be no less than 10.37 to guarantee a reliable result. And if conditions permit, a relatively higher SMR is preferred in practical scenarios. On the other hand, the approach presented in this paper is to highlight the fault anomaly of the planetary gearbox instead of the automatic identification of the fault source. Actually, the gears with different rotating frequencies are separately analyzed to achieve the overall monitoring of the planetary gearbox. In this process, due to the inhibiting effect of MTSA to asynchronous components, the extracted feature can uniquely indicate the health status of its associated gear, which enables the MTSA-PRPCA to diagnosis the planetary gearbox.

## 5. Conclusion

Based on the encoder signals, a novel anomaly detection algorithm is presented and validated in this work for the health monitoring of the planetary gearbox. The built-in rotary encoder provides an alternative information source for the condition assessment of the planetary gearbox and presents its advantage on low-costing and weak features extracting. According to the low-rank property of the regular component as well as the sparsity of fault anomaly, the RPCA model can be employed for anomaly separation, and the constraint of local periodicity in PRPCA further enhances its ability to extract a periodic anomaly. Besides, the discussed parameters have achieved good results on both simulation and practical signals, which provides a guidance for the further research on the applications of RPCA. However, it should be noticed that the presented approach is under the assumption of a stationary condition. When the machine is operated under the non-stationary condition, appropriate order tracking methods are expected to be constructed firstly to accurately transform the signal into an angular domain.

## Acknowledgment

This project is supported by the National Natural Science Foundation of China (Grant Nos. 51421004, 51875434) and the Defense Industrial Technology Development Program (Grant No. JCKY2018601C013), which is highly appreciated by the authors.

## Appendix

The optimal solution of equation (10) can be obtained by alternately optimizing $\mathbf{L}$ and $\mathbf{S}_0$, which is also known as alternating direction method of multipliers (ADMM). Firstly, $\mathbf{S}_0$ is fixed to update $\mathbf{L}$ as

$$\begin{aligned}
\hat{\mathbf{L}} &= \arg\min_{\mathbf{L}} \|\mathbf{L}\|_* + \langle \mathbf{\Lambda}, \mathbf{M}-\mathbf{L}-\mathbf{CS}_0\rangle + \tfrac{\mu}{2}\|\mathbf{M}-\mathbf{L}-\mathbf{CS}_0\|_F^2 \\
&= \arg\min_{\mathbf{L}} \|\mathbf{L}\|_* + tr\left(\mathbf{\Lambda}^T(\mathbf{M}-\mathbf{L}-\mathbf{CS}_0)\right) + \tfrac{\mu}{2} tr\left((\mathbf{M}-\mathbf{L}-\mathbf{CS}_0)^T(\mathbf{M}-\mathbf{L}-\mathbf{CS}_0)\right) \\
&= \arg\min_{\mathbf{L}} \|\mathbf{L}\|_* - tr\left(\mathbf{\Lambda}^T\mathbf{L}\right) + \tfrac{\mu}{2} tr\left(\mathbf{L}^T\mathbf{L} - (\mathbf{M}-\mathbf{CS}_0)^T\mathbf{L} - \mathbf{L}^T(\mathbf{M}-\mathbf{CS}_0)\right) \\
&= \arg\min_{\mathbf{L}} \|\mathbf{L}\|_* + \tfrac{\mu}{2} tr\left(\mathbf{L}^T\mathbf{L} - (\mathbf{M}-\mathbf{CS}_0)^T\mathbf{L} - \mathbf{L}^T(\mathbf{M}-\mathbf{CS}_0) - \tfrac{2}{\mu}\mathbf{\Lambda}^T\mathbf{L}\right) \\
&= \arg\min_{\mathbf{L}} \|\mathbf{L}\|_* + \tfrac{\mu}{2} tr\left(\mathbf{L}^T\mathbf{L} - (\mathbf{M}-\mathbf{CS}_0+\mathbf{\Lambda}/\mu)^T\mathbf{L} - \mathbf{L}^T(\mathbf{M}-\mathbf{CS}_0+\mathbf{\Lambda}/\mu)\right) \\
&= \arg\min_{\mathbf{L}} \|\mathbf{L}\|_* + \tfrac{\mu}{2} tr\left((\mathbf{L}-(\mathbf{M}-\mathbf{CS}_0+\mathbf{\Lambda}/\mu))^T(\mathbf{L}-(\mathbf{M}-\mathbf{CS}_0+\mathbf{\Lambda}/\mu))\right) \\
&= \arg\min_{\mathbf{L}} \|\mathbf{L}\|_* + \tfrac{\mu}{2}\|\mathbf{L}-(\mathbf{M}-\mathbf{CS}_0+\mathbf{\Lambda}/\mu)\|_F^2
\end{aligned} \tag{A.1}$$

where $tr(\bullet)$ represents the trace of a matrix. Note that some constant terms are added or removed in this process, which makes no difference to the final result. Similarity, $\mathbf{S}_0$ can be updated as

$$\begin{aligned}
\hat{\mathbf{S}}_0 &= \arg\min_{\mathbf{S}_0} \lambda\|\mathbf{CS}_0\|_1 + \langle \mathbf{\Lambda}, \mathbf{M}-\mathbf{L}-\mathbf{CS}_0\rangle + \tfrac{\mu}{2}\|\mathbf{M}-\mathbf{L}-\mathbf{CS}_0\|_F^2 \\
&= \arg\min_{\mathbf{S}_0} \lambda\|\mathbf{CS}_0\|_1 + \tfrac{\mu}{2}\|\mathbf{L}-(\mathbf{M}-\mathbf{CS}_0+\mathbf{\Lambda}/\mu)\|_F^2 \\
&= \arg\min_{\mathbf{S}_0} \lambda\|\mathbf{CS}_0\|_1 + \tfrac{\mu}{2}\|\mathbf{CS}_0-(\mathbf{M}-\mathbf{L}+\mathbf{\Lambda}/\mu)\|_F^2 .
\end{aligned} \tag{A.2}$$

## ORCID iDs

Kaixuan Liang https://orcid.org/0000-0003-1171-4730
Jing Lin https://orcid.org/0000-0002-7670-1482

Chuancang Ding https://orcid.org/0000-0002-7610-5293

## References


[1] Sawalhi N and Randall R 2014 Gear parameter identification in a wind turbine gearbox using vibration signals *Mech. Syst. Signal Process.* **42** 368–76

[2] Lei Y, Kong D, Lin J and Zuo M J 2012 Fault detection of planetary gearboxes using new diagnostic parameters *Meas. Sci. Technol.* **23** 055605

[3] Lee J, Wu F, Zhao W, Ghaffari M, Liao L and Siegel D 2014 Prognostics and health management design for rotary machinery systems—reviews, methodology and applications *Mech. Syst. Signal Process.* **42** 314–34

[4] Sun R, Yang Z, Luo W, Qiao B and Chen X 2019 Weighted sparse representation based on failure dynamics simulation for planetary gearbox fault diagnosis *Meas. Sci. Technol.* **30** 045008

[5] Samuel P, Paul D and Darryll J 2005 A review of vibration-based techniques for helicopter transmission diagnostics *J. Sound Vib.* **282** 475–508

[6] Du Z, Chen X and Zhang H 2018 Convolutional sparse learning for blind deconvolution and application on impulsive feature detection *IEEE Trans. Instrum. Meas.* **67** 338–49

[7] Salameh J, Cauet S, Etien E, Sakout A and Rambault L 2018 Gearbox condition monitoring in wind turbines: a review *Mech. Syst. Signal Process.* **111** 251–64

[8] Chen X and Feng Z 2019 Time-frequency space vector modulus analysis of motor current for planetary gearbox fault diagnosis under variable speed conditions *Mech. Syst. Signal Process.* **121** 636–54

[9] Feng Z and Zuo M 2013 Fault diagnosis of planetary gearboxes via torsional vibration signal analysis *Mech. Syst. Signal Process.* **36** 401–21

[10] Marzebali M, Faiz J, Capolino G, Kia S and Henao H 2018 Planetary gear fault detection based on mechanical torque and stator current signatures of a wound rotor induction generator *IEEE Trans. Energy Convers.* **33** 1072–85

[11] Roy S, Mohanty A and Kumar C 2014 Fault detection in a multistage gearbox by time synchronous averaging of the instantaneous angular speed *J. Vib. Control* **22** 468–80

[12] Stander C and Heyns P 2005 Instantaneous angular speed monitoring of gearboxes under non-cyclic stationary load conditions *Mech. Syst. Signal Process.* **19** 817–35

[13] Resor B, Trethewey M and Maynard K 2005 Compensation for encoder geometry and shaft speed variation in time interval torsional vibration measurement *J. Sound Vib.* **286** 897–920

[14] Gómez F C and Pérez P A 2010 Discrete time interval measurement system: fundamentals, resolution and errors in the measurement of angular vibrations *Meas. Sci. Technol.* **21** 075101

[15] Bourdon A, Chesné S, André H and Rémond D 2019 Reconstruction of angular speed variations in the angular domain to diagnose and quantify taper roller bearing outer race fault *Mech. Syst. Signal Process.* **120** 1–15

[16] Li B, Zhang X and Wu J 2017 New procedure for gear fault detection and diagnosis using instantaneous angular speed *Mech. Syst. Signal Process.* **85** 415–28

[17] Li B and Zhang X 2017 A new strategy of instantaneous angular speed extraction and its application to multistage gearbox fault diagnosis *J. Sound Vib.* **396** 340–55

[18] Zhou Y, Tao T, Mei X, Jiang G and Sun N 2011 Feed-axis gearbox condition monitoring using built-in position sensors and EEMD method *Robot. Comput.-Integr. Manuf.* **27** 785–93

[19] Zeng Q, Zainab M, Shao Y, Gu F and Andrew B 2017 Planetary gear fault diagnosis based on instantaneous angular speed analysis *23rd Int. Conf. on Automation and Computing (ICAC)* pp 1–6

[20] Jiao J, Zhao M, Lin J and Zhao J 2018 A multivariate encoder information based convolutional neural network for intelligent fault diagnosis of planetary gearboxes *Knowl.-Based Syst.* **160** 237–50

[21] Pérez P A, Gómez F C and Zaghar L 2014 Characterisation of parallel misalignment in rotating machines by means of the modulated signal of incremental encoders *J. Sound Vib.* **333** 5229–43

[22] Didier R and Jarir M 2005 From transmission error measurements to angular sampling in rotating machines with discrete geometry *Shock Vib.* **12** 149–61

[23] Remond D 1998 Practical performances of high-speed measurement of gear transmission error or torsional vibrations with optical encoders *Meas. Sci. Technol.* **9** 347–53

[24] Braun S 2011 The synchronous (time domain) average revisited *Mech. Syst. Signal Process.* **25** 1087–102

[25] Zhao M and Lin J 2017 Health assessment of rotating machinery using a rotary encoder *IEEE Trans. Ind. Electron.* **65** 2548–56

[26] Vidal R, Ma Y and Sastry S 2005 Generalized principal component analysis *IEEE Trans. Pattern Anal. Mach. Intell.* **27** 1945–59

[27] Wright J, Ganesh A, Rao S and Ma Y 2009 Robust principal component analysis: exact recovery of corrupted low-rank matrices *Proc. Advances in Neural Information Processing Systems* pp 2080–8

[28] Cui Y, Leng C and Sun D 2016 Sparse estimation of high-dimensional correlation matrices *Comput. Statist. Data Anal.* **93** 390–403

[29] Lin Z, Chen M and Ma Y 2010 The augmented lagrange multiplier method for exact recovery of corrupted low-rank matrices (Eprint arXiv) p 9 (arXiv:1009.5055)

[30] Cai J, Candes E and Shen Z 2008 A singular value thresholding algorithm for matrix completion *SIAM J. Optim.* **20** 1956–82

[31] Zhao M, Jia X, Lin J, Lei Y and Lee L 2018 Instantaneous speed jitter detection via encoder signal and its application for the diagnosis of planetary gearbox *Mech. Syst. Signal Process.* **98** 16–31

[32] Li Q and Liang S 2008 Multiple faults detection for rotating machinery based on bicomponent sparse low-rank matrix separation approach *IEEE Access* **6** 20242–54

[33] Xu X, Zhao M, Lin J and Lei Y 2016 Envelope harmonic-to-noise ratio for periodic impulses detection and its application to bearing diagnosis *Measurement* **91** 385–97